Energy 333 (2025) 137332

Contents lists available at ScienceDirect

Energy

journal homepage: www.elsevier.com/locate/energy

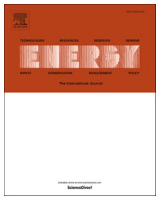

Assessment and optimal sizing of ice energy storage systems in various non-residential building types

Marco Griesbach [a,*], Andreas König-Haagen [a,b], Florian Heberle [a], Dieter Brüggemann [a]

[a] Chair of Engineering Thermodynamics and Transport Processes (LTTT), Center of Energy Technology (ZET), University of Bayreuth, Bayreuth, 95440, Germany
[b] ENEDI Research Group, University of the Basque Country – UPV/EHU, Bilbao, Spain

ARTICLE INFO

Keywords:
Ice energy storage
Heat pump
Optimization
Dimensioning
Non-residential building
Waste heat

ABSTRACT

Efficient heating and cooling solutions are essential to address climate change and rising energy costs. In non-residential buildings, low-temperature waste heat remains unused due to the lack of technical solutions. A promising approach is to combine this waste heat for heating and cooling. However, the temporal mismatch between waste heat availability and demand requires high-capacity thermal storages. Ice-energy-storage-systems (ICES) provide a viable solution, though no standards exist for their evaluation, design and sizing due to complex interactions with other supply units. A detailed numerical evaluation of ICES for various building types is conducted via a novel two-stage screening and optimization approach. Different configurations, with/without a CHP are optimized. The evaluation covers economic, environmental and social costs under different technological and regional boundary conditions. The methodology from a case study is applied to twelve model buildings. Simplified simulations identify potential candidates, followed by detailed computations to determine the optimal system configuration. High gas-to-electricity price ratios and low CO_2-emissions favor storage integration. ICES reduce CO_2-emissions by up to 55 % and lower demand-related costs. Substantial heating and cooling demand, with at least 8 % simultaneity, is needed to offset the investment. The methodology can be extended to other buildings, such as data centers or mixed-use districts.

1. Introduction

The increasing impacts of climate change and the rising costs of energy, particularly fossil fuels, are driving the need for more efficient and sustainable building energy supply solutions. The building sector currently accounts for nearly one-third of global final energy consumption [1] and approximately 37 % of global CO_2 emissions when considering both construction and operational phases [2]. According to the International Energy Agency (IEA), these figures are expected to rise further, as the annual growth in floor area of 2.5 % has consistently outpaced the reduction in energy consumption per square meter, which has only decreased by 0.5–1 % annually since 2010 [3]. In addition to heat provision, the demand for cooling has become increasingly important. Between 1990 and 2019, cooling-related CO_2 emissions nearly tripled [4]. The IEA projects that space cooling will continue to be the fastest-growing energy demand in buildings, with an annual growth rate of over 3 % for the next three decades, a rate that is eight times higher than the historical growth rate of heating demand over the past 30 years [5]. Moreover, many non-residential buildings harbor significant untapped potential for low-temperature waste heat recovery, such as from servers or other equipment. However, the lack of appropriate technical solutions currently limits its exploitation [6]. Consequently, there is a pressing need for innovative approaches that efficiently address both heating and cooling demands in buildings while balancing economic viability and ecological sustainability.

The concept of combining heating and cooling by utilizing waste heat generated within buildings offers significant potential for reducing energy consumption. However, Ghoubali et al. [7] emphasize the challenge posed by the low correlation between simultaneous heating and cooling demands, which is often a result of their temporal discrepancy in real buildings. Additionally, the interactions within the supply system are complex, and the low temperature level of waste heat further restricts the selection of suitable storage materials. Consequently, storage systems have recently garnered more research attention as a solution to address this temporal imbalance. Despite these advancements, waste heat recovery remains less widespread in the

This article is part of a special issue entitled: ECOS2024 published in Energy.

* Corresponding author.
E-mail addresses: marco.griesbach@uni-bayreuth.de, lttt@uni-bayreuth.de (M. Griesbach).

https://doi.org/10.1016/j.energy.2025.137332
Received 31 January 2025; Received in revised form 29 May 2025; Accepted 27 June 2025
Available online 3 July 2025

building sector compared to its application in industrial processes due to these limitations [7].

Extensive research has recently focused on enhancing the efficient use of waste heat in the building sector to increase its contribution to energy supply. Wang et al. [8] demonstrated that combining a heat pump with a ground source system improves the utilization of industrial low-temperature waste heat. Similarly, Egging-Bratseth et al. [9] showed that seasonal ground source systems can reduce costs and emissions. Li et al. [10] highlighted that using data center waste heat with a water tank and ground source storage can lower campus heating system operating costs by 6 % and CO_2 emissions by 8 %. A key focus of these studies is the reliance on geothermal boreholes due to their high storage capacity, despite the associated costs and increasing regulatory restrictions in a lot of countries.

Latent heat storage systems offer a promising alternative by leveraging the phase change process to achieve high energy density. Among various phase change materials (PCMs), water stands out as a cost-effective and environmentally advantageous option. It is cycle-stable, non-toxic, non-corrosive and non-flammable [11]. These unique characteristics have recently led to a surge in interest in ice energy storage systems within the building sector.

In recent years, there has been a growing focus on implementing stand-alone ice energy storage systems without the reliance on borehole support. Early studies conducted in 1980 by Shipper [12] demonstrated the feasibility of utilizing waste heat from refrigeration systems in residential buildings for combined heating and cooling. Later, Philippen et al. [13] developed a compact ICES for a multi-family residence in Switzerland, where both solar thermal energy and waste heat from the exhaust air of the ventilation system were used for storage regeneration. Additional studies expanded the use of ICES to various types of buildings, including residential houses [14], multi-family units [15], and kindergartens [16], primarily for heating purposes. Similarly, ICES have been explored for cooling applications in office buildings [17], healthcare facilities [18], mixed-use properties such as hotels and shopping centers [19] and districts [20–22]. However, these studies generally addressed heating and cooling demands as separate needs, rather than considering them as an integrated system. For the first time, an ICES with a volume of 500 m^3 was thoroughly analyzed for its ability to provide heating and cooling to a research building, accompanied by the development of a corresponding numerical model by Griesbach et al. [23]. A follow-up study [24] concentrated on optimizing both the operational strategies and the system design.

Ice energy storage systems are commonly combined with various heating and cooling technologies, leading to intricate interdependencies. As demonstrated in detail by Henn et al. [25], these interrelations also significantly affect the sizing of the storage system. In non-residential buildings, both the magnitude and timing of heating and cooling demands can vary significantly between facility types. Designing an ICES involves three key degrees of freedom—storage volume (capacity), charging-pipe length (charge power) and discharging-pipe length (discharge power)—each of which impacts technical performance, investment costs and operating expenses. Moreover, optimal storage configurations are tied to dynamic boundary conditions such as changing electricity prices and CO_2-emission factors, so that even identical buildings can require fundamentally different designs under different economic or ecological scenarios. Consequently, the design, evaluation and optimization of integrated heating and cooling solutions require an in-depth analysis of system performance through systematic parametric studies. This necessitates a versatile and rigorously validated model that can be used for comprehensive system simulations. While empirical guidelines exist for sizing ICES in residential buildings with relatively uniform heating and cooling needs, there is still a lack of systematic investigations for the implementation of ICES in different non-residential buildings. Existing studies are typically limited to individual case studies and do not cover a broad range of building types or sizes. Moreover, no study to date has evaluated such systems under varying economic and ecological boundary conditions, which are essential when assessing performance and feasibility across diverse non-residential applications.

To address this gap, this study expands upon the previously validated methodology for optimizing the implementation of an ICES, applying it to twelve model buildings. A combined heat pump-ice storage system with simultaneous charging and discharging is analyzed, deliberately excluding the solar support typically utilized in such systems. This represents a novel approach that aims to maximize the potential for utilizing waste heat generated within the building, thereby eliminating the need for additional solar thermal installations. It addresses the frequent competition of limited roof space in non-residential buildings, where photovoltaic systems are often prioritized over solar thermal collectors. Initially, simplified preliminary simulations were systematically conducted to identify appropriate building types and system configurations under varying conditions. Capturing this vast space of possibilities with simulations alone would entail prohibitive computational effort. Therefore, in this work we introduce, for the first time, a two-stage methodology that systematically combines i) simplified pre-simulations for rapid candidate screening with ii) detailed optimization and multi-criteria evaluation across a broad spectrum of non-residential building types, sizes and boundary conditions. Following this, optimization calculations were carried out exclusively for the selected scenarios. Subsequently, detailed variational simulations were performed to determine the optimal configuration for both the plant and storage. A downhill simplex algorithm was used to optimize the sizing of the plants for different configurations, including those with and without a combined heat and power (CHP) system. The evaluation was carried out using a multi-criteria approach, considering economic, environmental and social cost factors across a range of boundary conditions.

2. Description of the system

In the present study, the configuration of the system from a prior detailed publication [24] is employed in the context of other building types. In the preceding case study, a detailed examination of the supply system in the Technology Alliance of Upper Franconia (TAO) research building was conducted, which accommodates the Center of Energy Technology (ZET) among other facilities at the University of Bayreuth. The total area of the building is 5600 m^2, with 4000 m^2 allocated for laboratories and workshops. As domestic hot water is not a necessity in the NRB, the heat demand is predominantly associated with space heating. The cooling demand encompasses ventilation, cooling and machine cooling utilizing the laboratory cooling water network. A thorough delineation encompassing all nominal capacities can be found in another previous publication [23]. In that work, the ICES is delineated in detail along with a model of it that is developed and investigated. Furthermore, the comprehensive system, inclusive of all installed peripherals, is thoroughly examined and optimized with respect to operation and dimensionality in the context of various constraints. However, the present publication employs this validated methodology for the first time with a variety of different NRBs.

The primary objective of the supply system involves the implementation of a combined heat pump and an ice energy storage system which utilizes the waste heat produced within the building. This system functions as a link between the heating and cooling supply systems of the building. The heat pump (HP) is integrated into the return flow line of the heat distribution grid of the building, thereby reducing the load on downstream heat producers, such as a gas boiler (GB) and a gas-fired CHP unit, through the process of preheating the return flow. The brine side of the HP is connected to the ice storage, which functions as an energy source. The storage is regenerated using the cold water over a plate heat exchanger (HE CH) distribution system, thus also supporting the cooling needs. This distribution system also functions as a direct heat source for the HP via an additional plate heat exchanger (HE HP) during concurrent heating and cooling operation. In addition, a compression

chiller (CC) is employed, which is coupled with a dry cooler (DC) for the purpose of re-cooling. Under favorable ambient temperatures, the DC can be utilized for direct cooling via the plate heat exchanger, a process referred to as free cooling (FC). In order to account for the complex interactions between the various components within the system, the numerical model incorporates all the aforementioned components. For a comprehensive overview of the hydraulic implementation, refer to Ref. [24].

In this study, four cases are examined, as illustrated schematically in Fig. 1 C(I) denotes the realized configuration of [24] without the possibility of FC. In the reference case C(r), FC is applied instead of the HP and ICES. The cases G(I) and G(r) are analogous, in comparison to the C cases, due to the exclusion of the CHP.

The application of twelve distinct model buildings is employed, with a new building incorporated in each instance. The corresponding useable building area is retrieved from the model database in accordance with the methodologies outlined in Refs. [26,27]. The set of buildings under consideration constitutes 57.8 % of the total non-residential building stock in Germany in the year 2021, as indicated in Ref. [28]. Moreover, the Green Hospital Lichtenfels (GHL) [29] is regarded through a comparative lens, examining the methodologies employed in the calculation of synthetic load profiles and their correlation with real consumption data.

2.1. Numerical model

The focus of this work lies on the ice energy storage system with a heat pump. Therefore, a detailed numerical model from an earlier publication [23] is utilized. The mathematical basis for calculating transient systems is provided by the general transport equation [30], from which the energy conservation equation for describing latent thermal stores can be derived:

$$\frac{\partial(\rho cT)}{\partial t} + div(\rho \vec{u} cT) = div(\lambda \cdot gradT) + S_H \tag{1}$$

It includes the density ρ, the specific heat capacity c, the temperature T, the time t, the flow velocity field in x-direction $\vec{u}$, the thermal conductivity λ and the source term S_H. The phase change enthalpy L is considered as a function of the proportion of liquid phase γ therein. As the mass transfer in the liquid phase is not explicitly described for simplification and constant material properties are assumed, equation (1) can be expressed with the thermal diffusivity a:

$$\frac{\partial T}{\partial t} = a \cdot \nabla^2 T + S_H \tag{2}$$

The source term can be expressed in simplified form:

$$S_H = -L\rho\left(\frac{\partial \gamma}{\partial t}\right) \tag{3}$$

Thus, the temperature $T(h)$ can be determined using the specific enthalpy, while the temporal change of the enthalpy is determined from the second local derivative of the temperature:

$$\frac{\partial h}{\partial t} = \lambda \cdot \nabla^2 T(h) + S_H \tag{4}$$

However, instead of a defined melting point, a melting range with the apparent heat capacity c_{app} [31] is assumed:

$$c_{app} = c_{sen} + c_L \tag{5}$$

For this purpose, the sensible and latent heat capacity c_{sen} and c_L are used. Within the melting range, a continuous error function is applied to determine the liquid phase γ, which is zero in the solid phase and one in the liquid phase [32]. In combination with the error function, can be described as a continuous apparent heat capacity. By connecting the enthalpy method from equation (4) with the apparent heat capacity (5), the source term S_H is no longer necessary, whereby the energy conservation equation can be simplified as follows:

$$\frac{\partial h}{\partial t} = \lambda \cdot \nabla^2 T(h) \tag{6}$$

The heat transfer processes in the numerical implementation are described in a quasi two-dimensional model. Thereby, the heat transfer in the storage material is only considered vertical to the flow direction. Only through the HTF the heat transfer takes place parallel to the flow direction. The equation (6) gives the following equation with radius r for models in cylindrical coordinates:

$$\frac{\partial h}{\partial t} = \left(\frac{1}{r}\right)\frac{\partial}{\partial r}\left(\lambda_r \frac{\partial T}{\partial r}\right) \tag{7}$$

The discretization is carried out using the method of lines [33]. In this way, only the local derivatives of the equations are discretized by hand, resulting in a system of time-dependent ordinary differential equations that can be solved using methods already implemented in MATLAB Simulink. The adaptable, quasi-two-dimensional discretization in cylindrical coordinates is performed using the finite volume method (FVM) - described, for example, in Versteeg and Malalasekera [30] or Patanker [34] - and is implemented in the so-called C-mex s-functions. A detailed description of the discretization can be found in an earlier publication [23].

The heat transfer coefficient for the inside of the pipe is calculated using the Nusselt number Nu for a spiral pipe, which takes centrifugal forces into account [35]. The natural convection inside the PCM is included by an effective thermal conductivity λ_{eff}, using the correlation of Churchill and Chu [36] for free convection on a horizontal circular cylinder.

In order to account the surrounding soil, the ground temperature is used with the correlation described by Kusuda and Achenbach [37], while the storage capacity of the ground is neglected. Only heat conduction to the surrounding soil is included for simplicity, while losses at the top of the storage tank are neglected.

As the application of apparent heat capacity methods may result in significant discrepancies [38,39], a comprehensive validation process, inclusive of parameter variations, is conducted in Ref. [23]. The

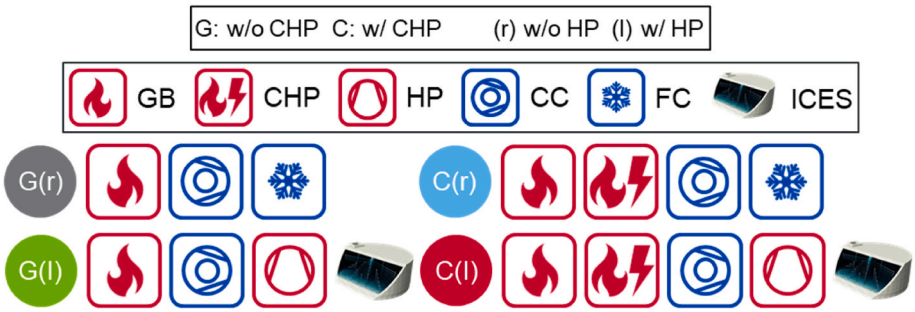

Fig. 1. Overview of the considered combinations.

numerical model is validated analytically against the exact solution of the Stefan Problem in Cartesian coordinates and the quasi-stationary solution in cylindrical coordinates. Furthermore, the simulation results are compared with long-term monitored data from a 500 m^3 ICES, recorded at 1-min intervals over a one-year period. In addition to the energy entering and leaving the storage, the state of charge is measured by a radar sensor, as well as the temperature at 30 measuring points within the storage volume and all supply lines. Given that the model is adaptable with regard to its dimensions, it can be employed within this study to examine the impact of storage dimensioning.

A model for the entire supply system on the generation side has been implemented in MATLAB [40] Simulink [41] utilizing the CARNOT library [42] which has already been compared with real data in an earlier publication [24]. The models are parameterized based on the data sheet specifications of the corresponding components.

In terms of heating, a gas condensing boiler, a gas-powered CHP unit and a heat pump are included. All models originate from the component library mentioned [42] and are partially extended. The model of a gas condensing boiler can be discretized on the heating water side as desired and is adopted unchanged. The CHP model calculates the mass flow m and the flow temperature T_{VL} as a function of the return temperature T_{RL} and the heat output $\dot{Q}_{th}$, where c_p corresponds to the heat capacity:

$$T_{VL} = T_{RL} + \frac{\dot{Q}_{th}}{\dot{m} \cdot c_p} \tag{8}$$

The gas consumption $\dot{Q}_{gas}$ for different partial load efficiencies is calculated as a function of $\dot{Q}_{th}$ using the thermal power factor f_{Q_th} according to the manufacturer's specifications:

$$\dot{Q}_{gas} = f_{Q\_th} \cdot \dot{Q}_{th}. \tag{9}$$

As opposed to the linear calculation of the electrical power P_{el} in the original model of the library, the electrical power factor f_{P_el} is used analogously for the calculation using a lookup table:

$$P_{el} = f_{P\_el} \cdot \dot{Q}_{th} \tag{10}$$

The dynamic behavior of a heat pump is described by an empirical model developed by Schwamberger [43], which is provided in Ref. [42]. It is based on the stationary characteristics of a heat pump in accordance with DIN 8900 [44]. Unlike the linear approximation of the primary, secondary and electrical power in the original model, the model is extended to include lookup tables with manufacturer specifications. These are used to determine the three variables as a function of the inlet temperature on the primary side and the outlet temperature on the secondary side.

On the cooling side, in addition to the ICES, a compression chiller and the possibility of free cooling through its recooling unit at low ambient temperatures are considered. As the compression chiller can also be regarded as a heat pump from a thermodynamic perspective, the existing model is adopted unchanged, with manufacturer specifications being used to parameterize the numerical model.

The electrical power consumption $P_{V,el}$ of the dry cooler is calculated using the power law for fans according to Wischhusen [45], which describes the operating behavior of the fans as a function of the air flow rate.

$$\dot{L} = \dot{L}_{nom} \cdot \left(\frac{P_{V,el}}{P_{V,nom}} \right)^{\frac{1}{f}} \tag{11}$$

Here, the prevailing air volume flow is $\dot{L}$, and $\dot{L}_{nom}$ is the nominal air volume flow while $P_{V,nom}$ is the electrical power consumption at the nominal point. A value of 2.9 is identified for the exponent f by approximating the manufacturer's specifications for the installed system. The fan model is connected to the unmodified model of a heat exchanger in the library using a control loop to set the required air flow rate.

In order to map the hydraulics and distribution, models of buffer tanks, pumps, valves and heat exchangers are taken unchanged from the library [42], whereby these are parameterized according to the manufacturer's specifications.

Subsequently, the real control mechanisms for pumps and valves are taken into account using PI control loops from standard Simulink [41] components.

Thus, analysis of the interconnected system can be conducted, taking all mutual interactions into account. The comprehensive model, including all components, is likewise verified through a comparison with measured data from a full year of the building's energy systems. Furthermore, the impact of varying operational modes is evaluated, along with an investigation of diverse optimization techniques concerning the operational performance. The optimal strategy identified in the previous step is adopted in this work. Furthermore, a consideration of subsequent system sizing can be found therein. In order to fulfill this objective, plants belonging to the same product series are approximated through the utilization of data sheet values on a similar basis. The same verified methodology is applied in this study to examine the effects of diverse plant configurations and sizes.

For a comparison between simulation and measurement, the coefficient of determination R^2 is used as a statistical criterion for evaluating the approximation.

$$R^2 = 1 - \frac{\sum_{i=1}^{n} \left(Y_{f,i} - Y_i \right)^2}{\sum_{i=1}^{n} \left(Y_{f,i} - \overline{Y} \right)^2} \tag{12}$$

Where Y_i represents the actual measured value and $Y_{f,i}$ is the estimated value from the model of n data points, where $\overline{Y}$ indicates the arithmetic average of Y_i.

2.2. Evaluation of the numerical results

The evaluation of the plant dimensioning and operation is conducted in accordance with economic and ecological parameters, in addition to a combined evaluation that includes social costs. The economic assessment employs the methodology delineated in VDI 2067 [46], whereby both single and recurring payments are included within a specified consideration period, known as an annuity. The recommendations given in this guideline are used regarding the observation period and system-specific parameters. Since this does not include ice energy storages, the characteristic values of borehole heat exchangers are used for service life and the other parameters, as in Vivian et al. [47] and Berger et al. [48]. The Chemical Engineering Plant Cost Index (CEPCI) [49] is employed within this study to enable the comparison of investment costs for the given plants on the same reference year. A comprehensive overview of the financial aspects and specifications can be found within [24]. In the detailed system simulation presented in section 3.4, the cost function from the aforementioned publication for the ICES is employed, utilizing the so-called six-tenths rule [50] with the default value of 0.6. In the preliminary simulations conducted in Section 3.3, the cost function $A_{0,ICES}$ underwent a simplification whereby it is expressed as a function of the heat extraction rate $\dot{Q}_{DC}$ rather than the storage volume as well as the heat exchanger pipe lengths:

$$A_{0,ICES} = 44,151 + 287,631 \left(\frac{\dot{Q}_{DC}}{100\ kW} \right)^{0.6} \tag{13}$$

In order to evaluate the ecological impact of the system, the emissions of CO_2 resulting from the consumption of gas and electricity, as well as the generation of electricity via CHP, are considered. The respective CO_2 factors for gas and electricity are employed herein, in accordance with the prevailing electricity supply mix of the grid. In accordance with [24], a subtraction using the grid factor is conducted

due to the fact that the total generated electricity is self-consumed. Furthermore, there is an overview of the parametric values of the benchmark cases representing Germany (DEU), the European average (EU27) and France (FRA). By employing these cases, this study aims to identify the impact of the imposed constraints on the assessment and optimization processes.

The challenge of a combined evaluation with several parameters is to ensure that the weighting is not arbitrary. As an example, Wang et al. [51] have weighted the energy, economic and environmental aspects of a heating, cooling and electricity supply system equally. However, for the planner or operator of such a system, monetary factors are usually decisive, although ecology is becoming increasingly important. Therefore, as described in detail in the previous publication [24], the cost rates recommended by the German Federal Environment Agency [52] for consequential climate damage caused by CO_2 emissions are used for a multi-criteria economic and ecological assessment. This damage cost rate can be used to estimate the amount of damage caused to society by greenhouse gas emissions from climate change. In this context, two distinct values for the social costs associated with CO_2 emissions are presented by Waldhoff et al. [53] in order to assess them economically. In a final step, the total system annuity is added to the total CO_2 emissions, which have been multiplied by the associated cost rates, resulting in a combined evaluation parameter.

2.3. Plant dimensioning optimization

This study examines the consequences of different system sizes and configurations, with the main focus on the ICES. As demonstrated by Wang et al. [54], the redundancy of a combined heating, cooling and electricity supply system is highly relevant. To ensure the security of supply, a certain degree of redundancy needs to be established. Consequently, the conventional heating and cooling plants must be capable of fulfilling the demand even without ICES in cases where the storage tank is fully charged or discharged. These components are defined according to standard procedures that are commonly applied in practice. The systematic limitation offers the benefit that the results and recommendations are linked to practical methods. In order to exclude the influence of different technologies on the results, only systems of the same series of the validated models are used. The selection is therefore reduced to technically available devices. In this context, two reference variants (r) and two variants with ICES (I) are considered, as illustrated schematically in Fig. 1. Within each variant, a scenario without CHP (G) and a scenario with CHP (C) are considered. In G(r) and C(r), FC is added, while in G(I) and C(I) it is omitted to maximize the utilization of waste heat via the ICES.

Initially, the input data, namely consumption data over a year, are loaded and analyzed. The conventional heating and cooling generators are then selected on the basis of this data. The Downhill Simplex method [55] is used to determine the optimal storage dimensioning. In order to reduce the simulation effort and thus the computing time, only the optimal operating strategy determined in an previous publication [24] is used under the assumption that the strategy also remains valid for other building types. During the execution of the algorithm, the storage volume and the ratios of pipe length per volume for the withdrawal and regeneration circuit are continuously varied. The volume essentially affects the storage capacity which is mainly important from a seasonal perspective, which is why annual simulations are carried out. The pipe length of the regeneration circuit, on the other hand, significantly influences the loading capacity. In addition to the withdrawal capacity, the pipe length of the discharge circuit also determines the ice layer thickness that forms on the pipes. Thus, by means of the optimization loop and the converged algorithm, the optimal storage can be determined, allowing a comparison with the reference cases.

2.4. Generation of synthetic load profiles for non-residential buildings

The calculation of the load profiles is carried out using the nPro software [56] which can be used as a planning tool for districts. The software is suitable for determining energy demand profiles for space heating, domestic hot water, air conditioning, process cooling, user electricity and electromobility. The demand profiles are calculated in hourly resolution by combining a base profile with a daily profile.

The base profile may be a constant value if there is no seasonal dependency as in the case of electromobility. On the other hand, electricity demand increases in the winter months due to the higher demand for lighting as a result of lower sunshine duration. A seasonal pattern is considered for domestic hot water, as the demand for hot water tends to be lower in the summer months. For space heating and air conditioning, the basic profile is related to the temperature of the ambient air. To account for the relevant difference of temperature between indoor and outdoor air, the degree day method [57–59] is applied. The degree day method is based on the assumption that the space heating demand rises linearly with the temperature difference between the ambient temperature and the set point indoor temperature [60]. Furthermore, the heating limit temperature, meaning the temperature beyond which the building is heated, is considered inside the model in relation to the building insulation standard as well as building-specific internal and solar gains. Likewise, the load demand for air conditioning is determined using the degree day method based on the cooling limit temperature. The limit temperatures are defined in an internal model database depending on the type and standard of the building.

It also contains the day profiles of the respective properties. A distinction is made between a working day, i.e. Monday to Friday, a Saturday and a Sunday. In addition, public holidays and school vacations are assigned to the weekday of the observation year and the time change from summer-to wintertime is considered by location. The underlying profiles as well as the values for the area-specific annual demand of the various building types are derived from several studies, experience from engineering offices and monitoring reports. The generated load profiles were validated for a variety of building types using real measured data [27,56]. In addition, a comparison with real consumption data from the new hospital building in Lichtenfels [29] is carried out as part of this study in Section 3.1. The values for the examined model buildings which are defined in Section 2 are listed in Table 1.

An analysis of the calculated consumptions is carried out by means of the following characteristic values of the heating and cooling demand. The absolute annual heating demand Q_h and cooling demand Q_c corresponds to the respective cumulative energy. As shown schematically in Fig. 2, the simultaneous energy Q_s represents the integral of the power of concurrent heat and cold.

In order to classify the results in terms of transferability to alternative building types, the characteristic values listed in Table 2 are used, which are calculated based on the annual simulation in nPro [56]. In this context, the ratio $R_{s/h}$ represents the correlation between the simultaneous energy amount to the total heat requirement, comparable to the ratio of simultaneous heating and cooling demand in Ref. [7]:

$$R_{s/h} = \frac{Q_s}{Q_h} \tag{14}$$

2.5. Preliminary simulation for selecting the cases to be examined

To determine potentially suitable building types in relation to the prevailing boundary conditions as well as the system configuration, a preliminary simplified simulation is first conducted in nPro [56]. As in each case just one building is considered, all losses are set to zero for the calculation of the thermal network. The simultaneity factor, which specifies the smoothing by the heating and cooling network between the peak load of the consumers and the energy center, is set to 1. The

Table 1
Specification and specific annual demand of the building types (new build).

Building	Specification	Specific annual demand in kWh/m²a				
		Space heating	Domestic hot water	Air conditioning	Process cooling	User Electricity
School small	School	68	3	21	12	12
School large	School	68	3	21	12	12
Consumer market non-food (NF)	Retail	74	3	25	2	78
Consumer market electronics store (EL)	Retail	74	3	25	2	78
Office small	Office	74	8	37	14	40
Office large	Office	74	8	37	14	40
Hotel small	Hotel	96	32	37	4	135
Hotel large	Hotel	96	32	37	4	135
Kindergarten	Kindergarten	79	3	17	0	12
Museum	Museum	74	5	29	0	37
Theater	Theater	85	6	12	0	69
Restaurant	Restaurant	85	50	17	0	128
GHL	Hospital	96	23	33	12	115

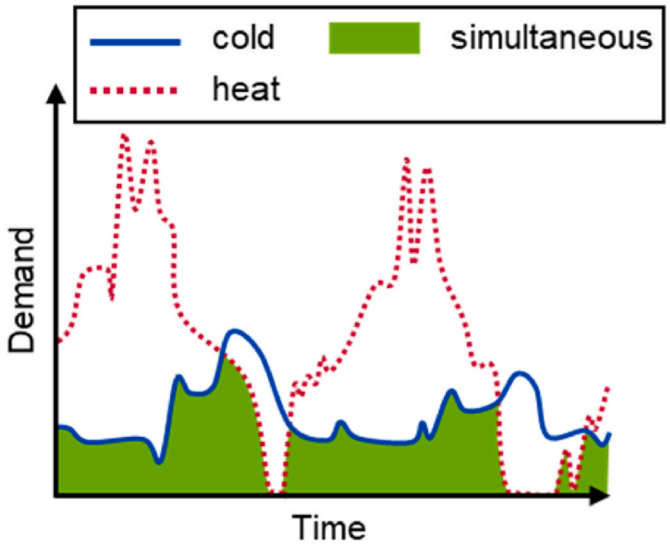

Fig. 2. Curve of the heating and cooling demand and the simultaneously occurring power.

Table 2
Floor space and consumption data analysis of the optimization results from nPro.

Building	Floor space in m²	Q_h in MWh	Q_c in MWh	Q_s in MWh	$R_{s/h}$ in (−)
School small	5003	355	165	41	0.11
School large	11,725	832	387	95	0.11
Consumer – NF	672	52	17	1	0.02
Consumer – EL	5400	416	146	15	0.04
Office small	1972	162	101	22	0.13
Office large	6998	574	357	78	0.14
Hotel small	2240	287	92	24	0.08
Hotel large	13,755	1760	564	143	0.08
Kindergarten	559	46	10	0	0.01
Museum	16,500	1304	479	31	0.02
Theater	6700	610	80	12	0.02
Restaurant	2500	338	43	19	0.06
GHL	24,502	2916	1103	661	0.23

calculation and optimization of the system design and operating simulation is carried out in the energy central. Established linear optimization methods are used for this purpose, which can be found in detail in Wirtz et al. [61]. Analogous to the rest of this paper, the annuity in accordance with VDI 2067 [46] is employed as the target function within the optimization process as described in section 0. To account for different price change factors, these are included in the base prices of the costs in advance. These serve as input data for the simplified simulation as the ecological parameters and the climate impact costs in the form of CO_2 costs. The investment costs of the systems are applied iteratively during system dimensioning.

Based on an energy balance of all relevant forms of energy in hourly resolution with constant efficiency levels, the simplified system simulation is carried out. Consequently, the performance will tend towards being overestimated with respect to the detailed time-variable model in MATLAB Simulink [40,41], where interactions between all the components are accounted for. In contrast to the detailed and computationally intensive ice storage model according to Ref. [23], the geothermal model of nPro [56] is employed in a simplified form. Basically, it is derived from an energy balance between the power drawn from a heat pump and the regeneration power supplied by the cooling loads. Since the principle of operation is thus identical to the one of an ice storage tank, it can also be used to model such a system according to the information provided by the manufacturer [56].

The process of selecting those variants that are potentially suitable for computationally intensive optimization calculations is shown schematically in Fig. 3. Initially, the respective building is defined from Table 1. Based on the default values provided, both the annual energy demand as well as the hourly load profiles for heating, cooling and electricity are determined. Furthermore, two reference simulations are carried out without ICES. As in Fig. 1 in each case a variant G(r) without and a configuration C(r) with CHP are used, for which an optimal dimensioning is identified. The procedure is carried out for the three constraints DEU, EU27 and FRA. It is then checked for each boundary condition whether the G(r) or C(r) variant leads to better results. Only for this optimum an iterative, optimized design is then carried out with ICES. The dimensioning of the remaining components from the reference simulation is not changed for reasons of redundancy and security of supply. Then the findings of the optimized ICES design are checked against the corresponding reference. If the implementation achieves an improvement compared to the reference, a calculation-intensive optimization of the storage dimensioning is conducted in section 3.4 for this building in accordance to the relevant constraints. Except for the ICES, it uses the same optimized system dimensioning of the preliminary simulation. Should the reference case turn out better than the ICES version, the case is rejected and not examined in detail, which saves unnecessary calculation capacity and time.

3. Results

3.1. Comparison of the developed synthetic load profiles using real measurement data

In a first step, the actual consumption data of the new hospital

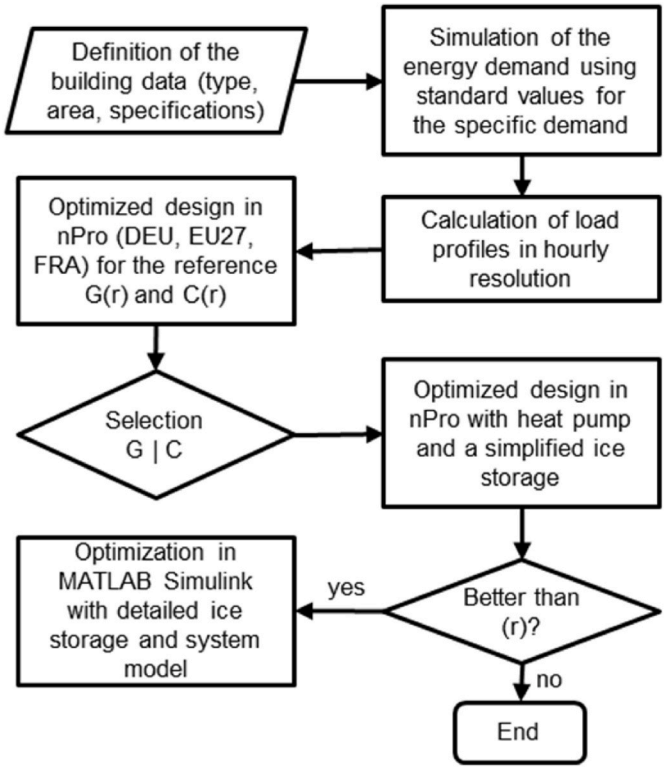

Fig. 3. Flow chart of the preliminary simulations to select the variants for optimized storage dimensioning.

building in Lichtenfels [29] is compared with numerically calculated values using the nPro [56] software. The period used is between 1st October 2020 and 30th September 2021. The data obtained from the hospital is intended solely as a point of comparison in order to verify the methodology employed. The subsequent variational calculations for alternative model buildings are derived exclusively from synthetic load profiles.

The required heat power is illustrated in Fig. 4. It can be seen that the curve is reproduced well. Especially at higher loads in the autumn and winter months, the two data sets are almost congruent in places. In the summer months, the actual consumption of the clinic usually exceeds the highly simplified numerically calculated values. Over the entire observation period, a coefficient of determination $R^2 = 0.94$ according to equation (12) results. The real total annual heat demand of 3050 MWh is compared to a numerically determined demand of 2916 MWh, corresponding to a difference of only around 4.4 %.

The curve of the required cooling power for both data sets is plotted in Fig. 5. While the peak load occurring in the summer months is almost identical, the commercial software noticeably underestimates the capacity in the winter months. The seasonal curve, on the other hand, is similar, resulting in a coefficient of determination $R^2 = 0.51$ according to equation (12). Similarly to the heating side, the seasonal differences are balanced out in an annual analysis. The real cooling demand of 1146 MWh is contrasted with a computed value of 1103 MWh, which is therefore only approx. 3.8 % lower.

For further analysis, Fig. 6 illustrates a comparison of the ordered duration lines of the heating and cooling demand. On the heating side, $R^2 = 0.96$ results according to equation (12), while on the cooling side a value of $R^2 = 0.78$ is obtained. The consumption in phases with high demand is overestimated in certain areas by the numerical model. This is largely offset in both cases by an underestimation in areas of low output.

In order to analyze the consumption data in more detail, Figs. 7–9 presents both data sets averaged hourly for three exemplary weeks. The weeks considered are a summer week, a winter week and a transition week, which are described in detail in an earlier publication [24]. In the summer week, the real data shows a significantly higher temporal fluctuation. The course of the cooling demand appears similar, particularly with regard to the maximum values. The real heating demand, on the other hand, is noticeably higher.

The course of the required heat load appears almost identical in the winter week. In contrast, the real cooling requirement clearly exceeds the values of the commercial software, although both are at a relatively low level.

The observation of the transition week shows the highest degree of correspondence for both heat and cold. While the real values have a higher fluctuation rate, their maximum and minimum values and the daily variation are highly similar.

In addition, the difference between the heating and cooling demand, which determines the proportion of heating and cooling occurring at the same time, agrees well on an annual basis. The seasonal pattern is very similar, resulting in a coefficient of determination $R^2 = 0.87$ according to equation (12). In total, the real data results in 947 MWh occur simultaneously, which corresponds to a $R_{s/h} = 0.31$ in accordance with equation (14). On the other hand, the numerically determined values are 661 MWh and a $R_{s/h} = 0.23$. By adjusting the ratio of process cooling to air conditioning and heating to domestic hot water within the nPro [56] software, the values could be approximated on a case-specific basis. This is deliberately omitted here, as the stored standard values, which reflect the respective building average, are used in further variation calculations for different buildings.

3.2. *Verification of the suitability of load profiles for storage optimization*

The methodology is verified through a comparison of the computing results by using synthetic and actual load profiles of the mentioned hospital building [29]. With both data sets, a detailed optimization is carried out in six different variants. This considers three different HP sizes, each with and without a CHP. Afterwards, the detailed optimized calculations in MATLAB [40,41] are compared with the simplified

Fig. 4. Measured (orig) and calculated according to nPro (syn) average daily heat demand of the GHL (1st October 2020–30th September 2021).

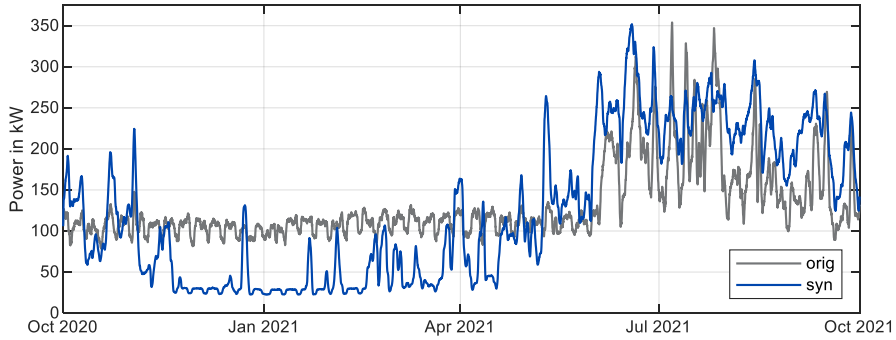

Fig. 5. Measured (orig) and calculated according to nPro (syn) average daily cold demand of the GHL (1st October 2020–30th September 2021).

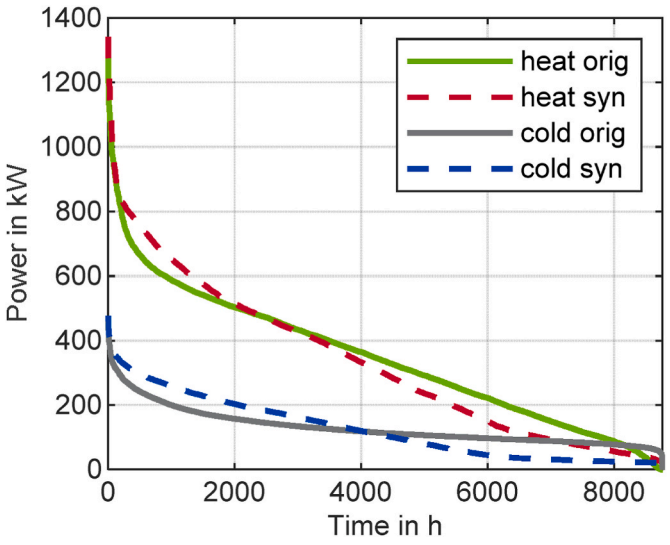

Fig. 6. Measured (orig) and calculated (syn) load duration curve according to nPro for the heating and cooling demand of the GHL (1st October 2020–30th September 2021).

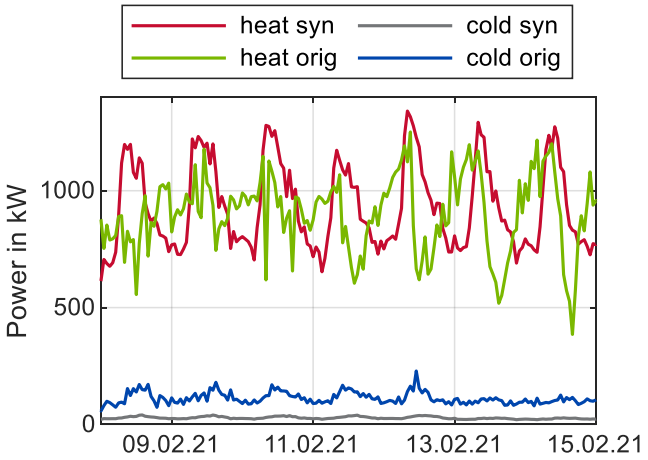

Fig. 8. Measured (orig) and according to nPro calculated (syn) hourly average heating and cooling demand of the GHL for a winter week (8th February 2021–14th February 2021).

simulations in nPro [56].

The ideal storage configurations that were determined are shown in Fig. 10. In the G cases, a configuration without and in the C cases with CHP are considered. With G(−), in which the smallest HP is examined, the volumes and the determined pipe lengths differ significantly. However, G(o) with a medium-sized HP and G(+) with the largest HP are

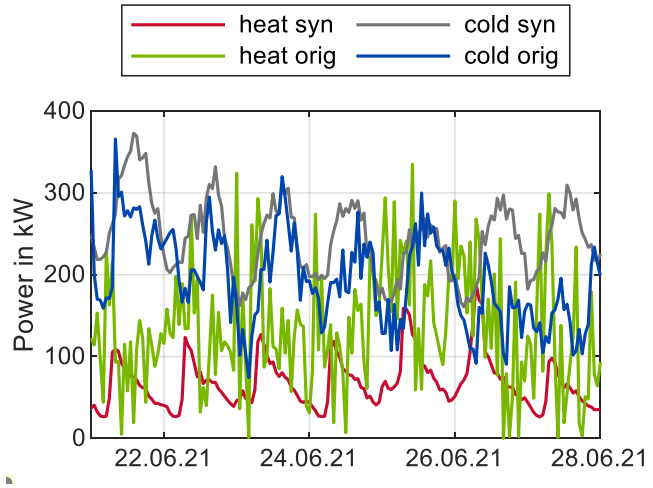

Fig. 7. Measured (orig) and according to nPro calculated (syn) hourly average heating and cooling demand of the GHL for a summer week (21st June 2021–27th June 2021).

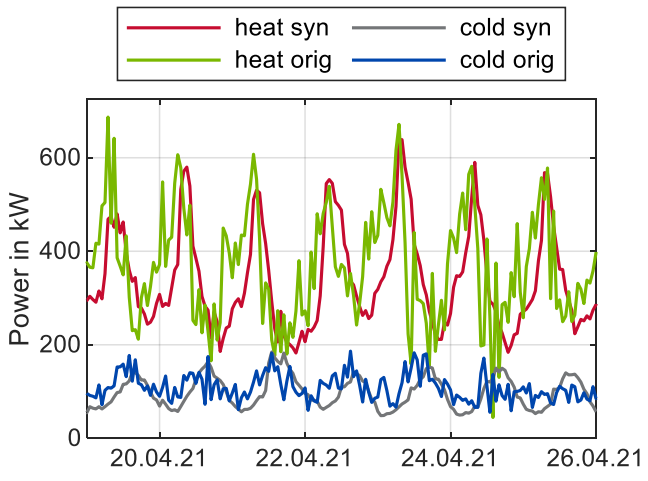

Fig. 9. Measured (orig) and according to nPro calculated (syn) hourly average heating and cooling demand of the GHL for a transition week (19th April 2021–25th April 2021).

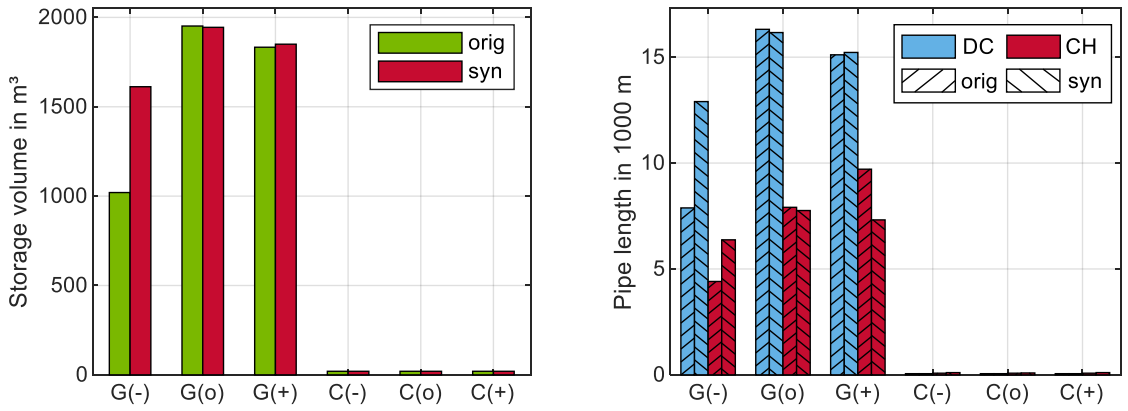

Fig. 10. Determined optimal storage volumes (left) and pipe lengths (right) for charging (CH) and discharging (DC) for all configurations of the optimization with real data (orig) and according to nPro calculated values (syn).

almost identical. In all C cases, the algorithm converges towards the lower limit of the variation range regardless of the HP size. Under the present boundary conditions, this mainly results from the fact that a larger dimensioning increases the runtime of the HP, which reduces the operating time of the CHP. Compared to this, the implementation of an ICES, which is associated with high investment costs, is not competitive in the examined case.

The potential ratios related to heating and cooling provisions, as well as the role of the ICES within the overall heating and cooling of the optimized variants, can be largely compared. It can be observed that the utilization of actual data in cases without CHP results in a cooling share that is approximately 29–40 % larger. The proportion of the dominant heat supply is highly comparable to the other cases, with a maximum deviation of 2–12 %. Consequently, the proportion of total generation is nearly equal, with a deviation of approximately 15–17 % for both data sets. In all C-cases, all proportions are almost negligible and identical.

Furthermore, a comparison of the resulting CO_2 emissions is presented. As expected due to the slightly different values for heating and cooling demand described above, this results in different absolute values. The progression as well as the arrangement of the variants is consistent across both data sets. Whether the data are real or synthetic, G (o) represents the optimal or best-case scenario.

For the economic evaluation, the annuities in total with the different climate impact cost rates are displayed in Fig. 11 for all cases. As the required energy amounts differ with both data sets, differences in absolute values can also be expected. Nevertheless, the order from optimum to pessimum is identical for all variants with both data sets. The reference case G(r) represents the worst case in a combined assessment, whereby the direct costs are better compared to the other G-cases due to the low investment. While the climate impact costs are low in these cases, the G-cases are not competitive with the C-cases in both purely economic and multi-criteria assessments. With both variants, G(−) with the smallest HP is in the best possible position, while the costs increase with the size of the HP. The C(−), C(o) and C(+) cases are almost identical with both load profiles, whereby the costs increase slightly with increasing HP size due to the higher investment costs required compared to the G cases. With both data sets, C(r) represents the best possible case overall. Compared to the C cases, the costs decrease as the additional investment for the ICES, which could only make a negligible contribution to the energy supply anyway, is eliminated. As free cooling is also used to generate cooling in this reference case, the climate impact costs are also lower.

Overall, it can be concluded that the optimization using real data is comparable to the numerically determined synthetic data sets. From the author's point of view, these can therefore be used to estimate the system configuration and storage dimensioning despite the differences described.

In a final step, the detailed optimization in MATLAB [40,41] is compared with a simplified simulation in nPro [56]. In both cases, the synthetic load profiles for the new clinic building in Lichtenfels are used. In contrast to the simplified simulation, the computationally intensive system simulation considers the dynamic system behavior, real control mechanisms, mutual interactions and the detailed behavior of the storage system.

A comparative analysis of the calculated storage sizes for the G-cases reveals that the simplified calculation generally identifies a configuration within a similar range. The lower bound of the variation range is selected as storage volume in all C-cases in both optimization

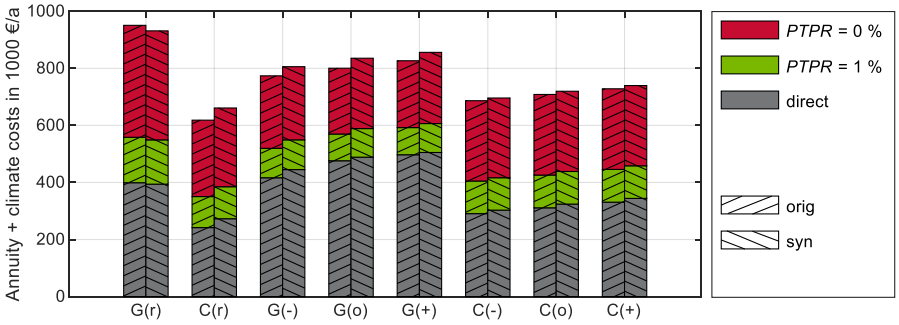

Fig. 11. Annuity and climate impact costs with different *PTPR* for all configurations of the optimization with real data (orig) and according to nPro calculated values (syn).

calculations. The proportion of the ICES allocated to the provision of heating and cooling in both simulation variants is, in general, an overestimation in the context of the simplified simulation. A contributing factor to this discrepancy is the omission of detailed consideration of mechanisms such as storage losses and interactive effects between the systems. The most significant distinction is that in nPro, a continuous output control of the HP is assumed, which notably extends its runtime and operational times. In the C-cases, all proportions are nearly identical and simultaneously minor in both simulation approaches due to the limited storage size. Consequently, it can be observed that the simplified simulation can be utilized to exclude these variants. With regard to the subsequent annual CO_2 emissions, the detailed calculations indicate that the values are significantly higher for all variants. This is largely due to the inclusion of additional factors, such as losses, operating restrictions, and partial load efficiencies.

The resulting economic viability and climate impact costs are shown in Fig. 12. Using both simulation approaches, G(r) is identified as the worst choice. G(+) is in second place in both versions, followed by G(o) and G(−) in the detailed simulation, while G(o) is better due to the increased use of heat pump in nPro as this results in lower CO_2 emissions. Independent from the degree detail of the simulation, the results for all C-cases with ICES are very similar, whereby the costs increase with the size of the heat pump.

In conclusion, an overestimation of the ICES contribution is evident in the simplified simulation, primarily due to the exclusion of intricate control mechanisms. As a consequence, the absolute values of production and the subsequent costs and CO_2 emissions may also vary. Nevertheless, a consistent approach to identifying and classifying the variants can be observed. Consequently, the simplistic and time-efficient modelling approach is well suited for preliminary estimation and selection, whereas the comprehensive system modelling considers all phenomena associated with full-scale plant operation.

3.3. Selection of the buildings

A comprehensive examination of the twelve model buildings classified into eight categories (section 2.4) is conducted to investigate a diverse range of non-residential buildings under varying boundary conditions. To this end, the environmental and economic boundary conditions of DEU, EU27, and FRA are employed for each of the selected buildings. A comprehensive analysis such as the detailed variational computations presented in the previous section (i.e., three different HP sizes each for one case with and one without CHP) may not be feasible at this stage due to an unacceptable increase in calculation time. A total of 216 highly-computational-intensive optimizations, in combination with 72 reference simulations, would necessitate a pure computing time of 48 months when executed in parallel on 44 threads. Furthermore, the time and resources devoted to the creation and evaluation of the model must be considered. Nevertheless, this would entail needless variants in which the inclusion of a CHP or ICES would be unprofitable and in which the optimization procedure would reach the specified minimum.

Accordingly, the methodology described in section 2.5 is employed in the following to determine suitable configurations through preliminary simulations. In order to conduct an enhanced sizing for the GB, the CHP and the CC across the 108 resulting cases, a simplified simulation in nPro [56] is employed. The design of the GB is identical for each respective building in G(r), regardless of location. This is due to the necessity of guaranteeing the reliability of supply via the single heat generator. In contrast, in cases C(r) and ICES, it is possible to identify different dimensions depending on the size of the CHP. In accordance with the redundancy requirements, a reduction of the GB size in conjunction with G(r) is not applicable for ICES. In all EU27 and FRA cases, the minimum CHP size is identified as the optimal selection, due to the lack of competitiveness of the CHP in comparison to the GB. The only exception to this is the "Hotel large" building, subject to the constraints of EU27. As a result, in the ICES instance, there is no evident CHP. In cases where CHP is present, its size aligns with that of variant C (r), which is attributed to redundancy considerations. For the same redundancy reasons, the CC size remains consistent across configurations as well as boundary conditions. In the cases G(r) and C(r), the CC serves as the sole cold generator.

The resulting selection between configuration G or C for the implementation of an ICES and its preliminary design based on nPro [56] is summarized in Table 3. Under the boundary condition of DEU, the combination with CHP is identified in nine and in three cases without CHP. In the case of EU27, only one building is configured with a CHP and none with FRA boundary conditions. The ICES design has specified an extraction power of 20 kW as the minimum requirement for the iterative optimization of the dimensions. In all cases under DEU

Table 3
Results of the preliminary simulation in nPro for selecting the variants.

Building	Reference simulation (G|C)			Preliminary design ICES in kW		
	DEU	EU27	FRA	DEU	EU27	FRA
School small	C	G	G	20	28	54
School large	C	G	G	20	130	172
Consumer market non-food (NF)	G	G	G	20	20	20
Consumer market electronics store (EL)	C	G	G	20	20	54
Office small	G	G	G	20	20	20
Office large	C	G	G	20	53	111
Hotel small	C	G	G	20	20	20
Hotel large	C	C	G	20	246	426
Kindergarten	G	G	G	20	20	20
Museum	C	G	G	20	305	450
Theater	C	G	G	20	20	20
Restaurant	C	G	G	20	20	20

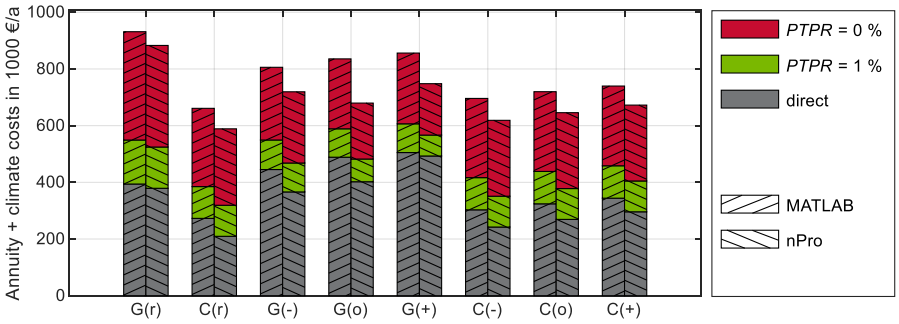

Fig. 12. Annuity and climate impact costs with different *PTPR* for all configurations of the optimization in MATLAB Simulink (MATLAB) and in nPro (nPro), each with load profiles calculated according to nPro.

boundary constraints, this minimum value is identified. In the case of the EU27, this limit value is found in seven out of twelve buildings, while in the case of the FRA, it is present in 50 % of the examined buildings.

An overview of the calculated annuity results in total with climate impact costs from the preliminary simulations is listed in Table 4. All combinations in which an ICES configuration represents an advantage compared to the reference are marked in bold. They are investigated in the following chapter using calculation-intensive variation computations. Under the boundary condition of DEU, no potentially suitable building is identified. In cases where the configuration with CHP is selected as the optimal reference, an additional ICES always leads to degradation. On the one hand, the investment costs increase, while at the same time the use of the HP leads to a displacement of the CHP as the basic load generator, which has high leverage from an economic point of view. In cases where G(r) performs better, the integration of an ICES is not profitable due to low energy quantities, as the potential savings cannot compensate for the high investments. Under the boundary condition of EU27, the cases "consumer market combined non-food module" and "kindergarten" are also excluded due to the generally low energy quantities. In addition, ICES integration in the buildings "Theater" and "Restaurant" leads to a degradation. This is mainly due to the particularly high time lag between heating and cooling consumption, as no process cooling is required, see Table 1. A similar pattern emerges under the boundary condition of FRA, whereby the "Theater" building with ICES performs better than the reference.

For the subsequent plant simulations, real available plants are employed. However, in nPro [56], the plant size is adjusted continuously, resulting in minor discrepancies in the plant sizing. The nominal capacities of the GB, the CC, the CHP, the HP and also the case designation used in the following are listed in Table 5. A comprehensive analysis is conducted in MATLAB with the available plants from the identical series as the validated models described in Ref. [24]. In each instance, the unit that most closely approximates the values from nPro is selected.

3.4. Results of the detailed simulation

The results of the detailed system simulation and optimization regarding the dimensioning are presented in the following. Using the optimization algorithm and the procedure described in section 2.3, the optimum storage dimensioning is identified for each of the configurations selected in the preceding chapter. An overview of the attainable proportions of the heating and cooling supply for all variants in the optimization process is provided in Fig. 13. Likewise, each of the identified optima is marked. As the dimensioning of the systems in accordance with Table 5 can vary with the boundary conditions, different combinations may result in certain cases. Due to varying dimensioning, there are differing variants between the "small" and "large" building sizes, despite the identical values for the specific annual demand according to Table 1.

Using the optimization algorithm and the procedure described in section 2.3, the ideal storage size is identified for each of the configurations selected in the previous chapter. The algorithm converges towards the specified lower limit of the volume of 20 m^3 in twelve cases. In six configurations, however, a volume is identified within the defined optimization interval, which tends to be larger under the RBD of FRA than in EU27. The cases include the buildings "School small", "School large", "Office large" and "Hotel large". Consequently, the examination is limited to buildings in which the storage integration performs better than the reference. Variants in which the integration is marginally superior should not be considered.

The feasible contributions to the heating and cooling supply vary depending on the type of building and, in some cases, its size. This can be explained by different plant sizes and the absolute heating and cooling requirements in each case. As a result, there may be different options between the "small" and "large" building sizes even though the values for the specific annual demand according to Table 1 are identical.

The energy amounts that can be achieved by the HP with the respective storage volume and their share of the total supply are shown in Fig. 14. Furthermore, the values of the CHP and the CHP are shown. The compositions for the corresponding reference case without ICES are also included. In the cases with minimal storage volume, the contribution of the heat pump is minimal. The storage volume of 20 m^3 as an energy source constitutes a hardly useable capacity for the heat pump. In addition, the low thermal capacity of the brine circuit on the primary side often leads to the heat pump being shut down due to low inlet temperatures, see Ref. [24]. The largest amount of approx. 53 % can be obtained under the boundary condition of FRA in case 2-F (see Table 4 for definitions), while the smallest amount of 15 % can be supplied in 2-E using the significantly smaller system within EU27. A similar behavior can be seen in the "Office large" scenario, where the HP can supply approx. 18 % in 5-E and approx. 43 % in 5-F. Although the algorithm converges towards the minimum for 1-F and the ICES is therefore barely useable, the HP can cover approx. 20 % of the demand with a relatively small storage tank in 1-E. By using the largest storage volume identified in 7-F for the "Hotel large" application, the HP can cover a fraction of approx. 37 %. The share of the ICES in 7-E is minimized by the minimum storage volume so the CHP running time is maximized. Except for 7-E, the heat supply in all reference simulations is provided entirely by the GB.

Similarly, the energy amounts and contributions of the ICES to the provision of cooling are shown in Fig. 15. In the variants where the algorithm converges towards the storage minimum, the contributions of the ICES are again very limited. Due to the low storage capacity, regeneration can hardly be used, as the storage is quickly completely melted and has an average temperature of more than 5 °C, see Ref. [24].

Table 4
The results of the annuity, including the climate impact costs of the preliminary simulation in nPro for the selection of variants.

Building	Annuity in sum with climate impact costs in €/a								
	DEU			EU27			FRA		
	G(r)	C(r)	ICES	G(r)	C(r)	ICES	G(r)	C(r)	ICES
School small (1)	152,313	150,478	154,019	148,470	158,905	**136,778**	142,874	158,905	**112,279**
School large (2)	342,975	278,818	291,127	333,307	354,257	**273,378**	321,363	348,625	**224,685**
Consumer – NF	26,359	28,409	36,041	26,005	33,689	33,637	25,534	36,082	30,785
Consumer – EL (3)	151,101	128,503	139,271	148,642	161,417	**143,002**	144,444	163,773	**122,304**
Office small (4)	76,168	77,689	79,029	73,334	85,080	**71,375**	69,665	86,234	**62,269**
Office large (5)	241,830	214,073	222,993	232,142	242,243	**205,395**	218,948	235,488	**164,260**
Hotel small (6)	101,428	88,294	96,842	100,160	109,642	**95,411**	97,285	113,704	**86,858**
Hotel large (7)	551,190	341,392	354,532	541,676	523,052	**440,129**	527,267	543,824	**330,068**
Kindergarten	24,916	34,410	37,149	24,900	39,083	36,011	24,719	41,072	34,538
Museum (8)	437,216	288,773	301,284	427,657	436,280	350,530	414,166	430,768	**276,614**
Theater (9)	177,713	123,634	135,311	178,935	188,296	179,822	179,154	195,728	**176,093**
Restaurant	105,387	84,621	93,829	106,537	115,312	112,337	106,829	123,314	110,078

Table 5
Dimensioning of the systems in nPro and MATLAB including all variants.

Case	Building	Nominal power in kW							
		GB		CC		CHP		HP (primary side)	
		nPro	MATLAB	nPro	MATLAB	nPro	MATLAB	nPro	MATLAB
1-E	School small	371	440	762	761	–	–	28	26.3
1-F								54	52.6
2-E	School large	870	900	1780	1784	–	–	130	131.6
2-F								172	169.2
3-E	Consumer market electronics store	276	350	366	366	–	–	20	17.0
3-F								54	52.6
4-E	Office small	218	270	200	207	–	–	20	17.0
4-F									
5-E	Office large	771	900	699	699	–	–	53	52.6
5-F								111	106.6
6-E	Hotel small	170	200	178	178	–	–	20	17.0
6-F									
7-E	Hotel large	837	900	1080	1053	142	140	246	253.8
7-F		1039	1100			–	–	426	426.4
8-E	Museum	633	700	1228	1231	–	–	305	319.8
8-F								450	426.4
9-F	Theater	365	440	207	207	–	–	20	17.0

Moreover, due to the low volume, the running times of the heat pump are limited and the cold water network can only rarely be used as a direct energy source for the HP by the HE HP. The maximum possible contribution to the cooling supply of approx. 27 % can be obtained from the ICES in case 1-E. In contrast to the heat supply, in scenarios 2 and 5 the proportion of the cooling supply can barely be increased by raising the storage volume. For instance, this amounts to approx. 19 % in cases 2-E and approx. 22 % in 2-F and approx. 17 % in 5-E compared to approx. 18 % in 5-F. This can be attributed in particular to the time lag between the heating and cooling demand. As a result, the cooled storage tank is heated by the surrounding ground and can therefore provide less cooling. In 7-F, this effect is maximized, due to the fact that the cooling demand in the "Hotel large" building is mainly due to air conditioning, see Table 1. The proportion of process cooling is very limited, leading to high losses to the ground as a result of the long time offset. The reference cases also consider the possibility of FC, which is not used in the configurations with ICES. In all combinations, the majority of cooling is provided by the electrically operated CC.

The resultant yearly CO_2 emissions are illustrated in Fig. 16. Based on the configurations with minimum storage size, the results of the reference simulations and the ICES cases are nearly similar. As shown in Figs. 14 and 15, ICES can only make a negligible contribution, which means that hardly any changes in CO_2 emissions are possible. In contrast, the most significant reduction of approx. 55 % compared to the reference can be seen in 2-F with a large storage tank. This can be attributed in particular to the high proportion of heat provided by the HP. For case 2-E, where the proportion accounted by cooling is almost identical, the improvement in terms of CO_2 emissions is limited to approx. 18 %, as the amount accounted by the HP for heating is clearly lower. A comparable pattern can be observed in the "Office large" building. While in 5-F the reduction is approx. 49 %, mainly due to the high contribution of the heat pump, in 5-E the lower share of HP with similar cooling provision only achieves an improvement of approx. 20 %. A similar trend can be found in case 7-F, in which the CO_2 emissions are reduced by approx. 40 % due to the noticeable contribution of the HP, although the proportion allocated to cooling is very limited. Compared to the reference, the smallest improvement of approx. 15 % can be observed in case 1-E, in which the largest possible share of cooling is provided. All in all, this indicates a predominant impact of heating on CO_2 emissions, while the influence of cooling takes on a subordinate position among the given boundary conditions.

In Fig. 17, the resultant annuity in connection with climate impact costs as described in Section 2.2 with different pure time preference rate *PTPR* is illustrated. This shows that the direct costs always increase due to the ICES implementation. Under the applied constraints, the increased investment is therefore not compensated for by a reduction of demand-related costs. Also in a multi-criteria evaluation with $PTPR = 1$ %, for all combinations the reference is ranked better. With $PTPR = 0$ %, on the other hand, the combined evaluation together with ICES can be favorable. This occurs in cases 5-E with an improvement of approx. 0.1 %, 2-F with approx. 6.2 % and 7-F with approx. 8.5 %. For the other cases, higher costs must be accepted despite useable storage capacity, regardless of significant reductions in CO_2 emissions.

To conclude, the buildings under consideration are plotted in Fig. 18 as a function of the annual heating and cooling demand and the $R_{s/h}$ according to equation (14). Based on the preliminary simulations from Section 3.3, some building types for which the integration of an ICES is not recommended can be eliminated. Further filtering is carried out through the detailed variation calculations to identify optimal storage dimensions, whereby the implementation of an ICES can be recommended from a multi-criteria perspective in four of the 12 examined buildings. This selection includes the types: "School small", "School large", "Office large" and "Hotel large". Each of the four buildings has the properties listed below in common, which therefore can be seen as a minimum criterion for ICES integration. The heat demand must be at least approx. 355 MWh per year. This minimum requirement is necessary to ensure that savings from a reduction in gas consumption and the climate impact costs according to section 2.2 can compensate for the higher investment. As a result, the capital and operating costs increase. Furthermore, the annual cooling requirement must be at least approx. 165 MWh. With lower heating or cooling needs, the combined assessment parameter is disadvantageous compared to the reference, particularly due to low investment costs without ICES. An additional common feature of the identified configurations is that the $R_{s/h}$ needs to be at least approx. 8 %. Higher values tend to be beneficial with regard to the efficiency and performance of the storage system compared to the

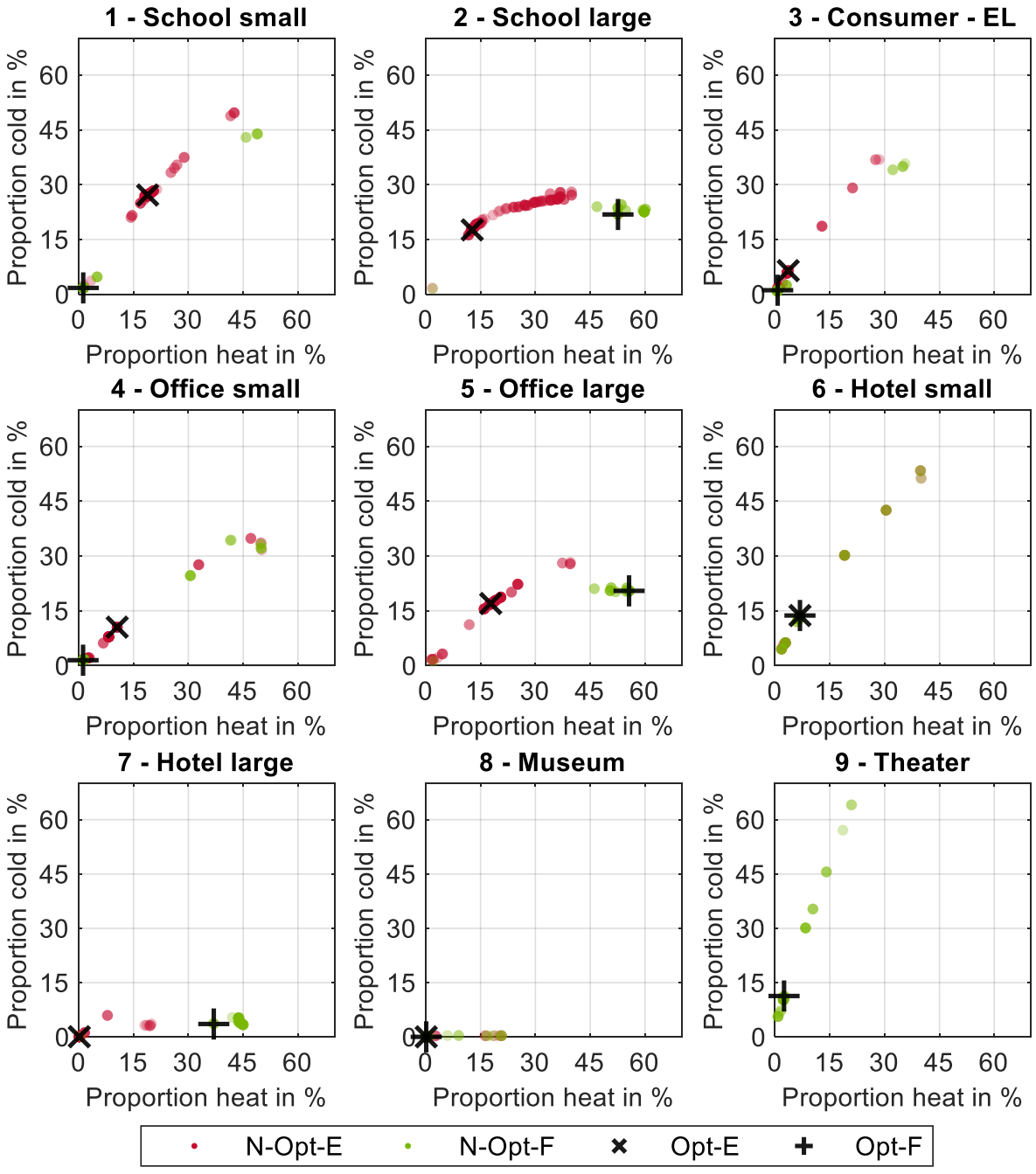

Fig. 13. Composition of the heat generation of the detailed simulations in MATLAB Simulink (absolute values above and relative values below) of the composite system of all pre-selected configurations with optimized ICES and the corresponding reference simulation.

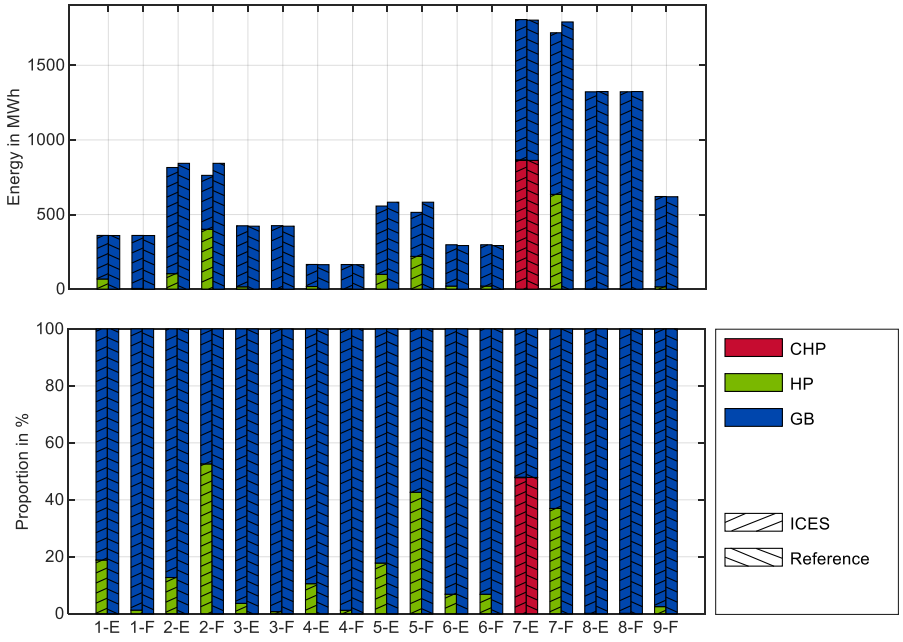

Fig. 14. Composition of the heat generation of the detailed simulations in MATLAB Simulink (absolute values above and relative values below) of the composite system of all pre-selected configurations with optimized ICES and the corresponding reference simulation.

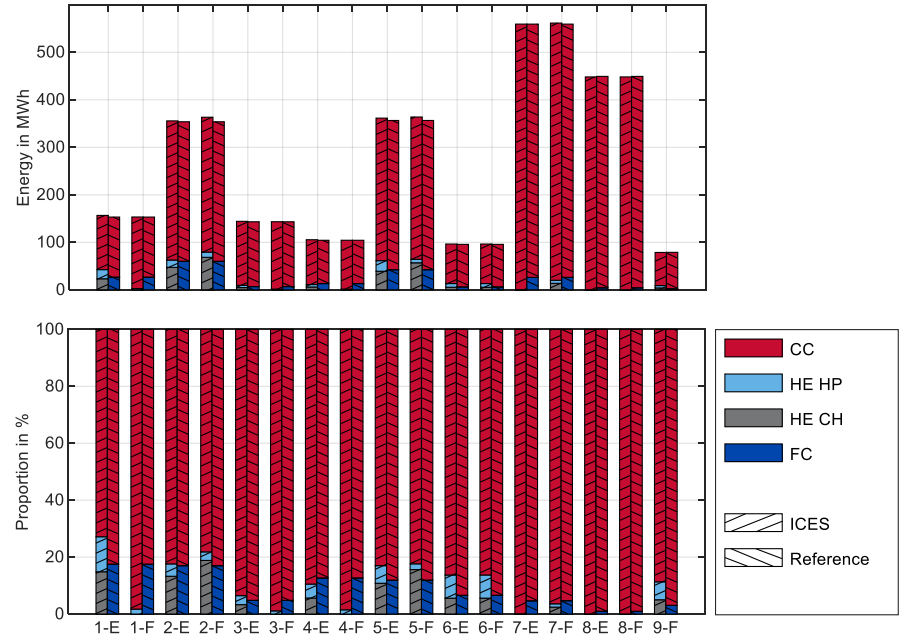

Fig. 15. Composition of the cold generation of the detailed simulations in MATLAB Simulink (absolute values above and relative values below) of the composite system of all pre-selected configurations with optimized ICES and the corresponding reference simulation.

reference. For one thing, it allows the cooling grid to be used more often as a direct energy source via HE HP, thereby increasing the inlet temperatures on the brine side of the HP and hence the efficiency of the HP. In addition, a smaller time shift between heating and cooling requirements decreases the required storage capacity and thus the investment costs can be reduced.

4. Conclusion

To address the challenges posed by climate change and rising energy costs, the development of more efficient heating and cooling solutions for buildings has become increasingly essential. Despite the growing interest, there are currently no established standards for the optimal design of ice energy storage systems in non-residential buildings due to the high variability in their applications. In this study, a systematic method for optimizing interconnected ICES has been proposed. This

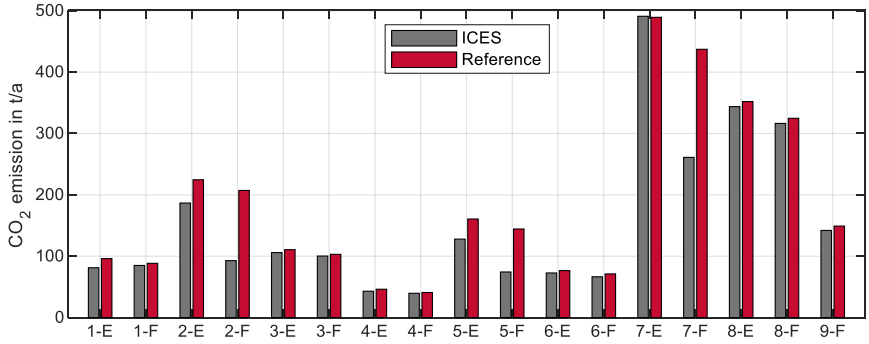

Fig. 16. CO_2 emissions in all configurations selected in advance in nPro for optimization with ICES as well as the reference simulation both in MATLAB Simulink.

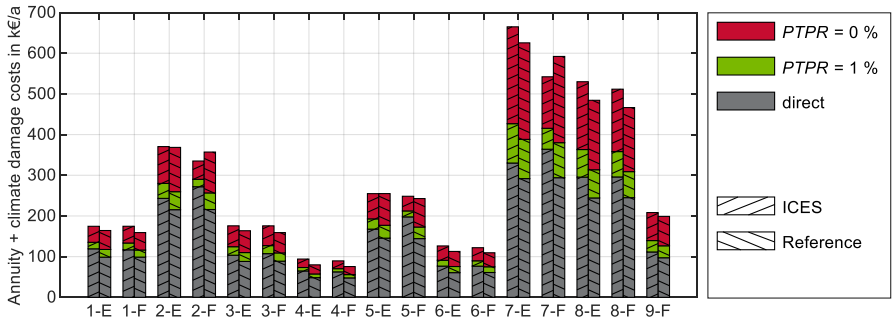

Fig. 17. Annuity and climate impact costs using different *PTPR* for the configurations selected in advance in nPro for optimization with ICES as well as the reference simulation both in MATLAB Simulink.

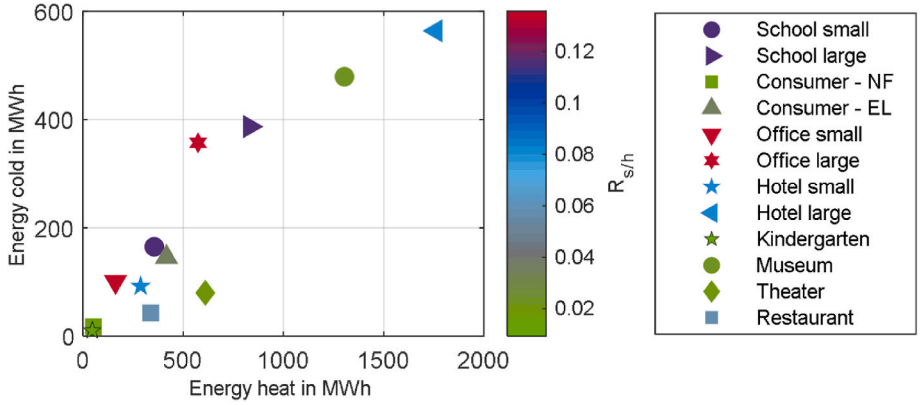

Fig. 18. Yearly heating and cooling energy demand as a function of $R_{s/h}$ for all buildings considered.

approach includes a multi-criteria evaluation encompassing economic and environmental assessments, along with a combined consideration of both through the integration of social costs. Additionally, the study examines the effects of various system configurations, including those with and without combined heat and power systems. The optimization process employed a downhill simplex algorithm to determine the optimal storage dimensions for each configuration, factoring in boundary conditions for environmental and economic parameters across Germany, France and the European Union. To extend its applicability, the methodology was applied to a large number of other non-residential building types.

For the first time, this methodology couples rapid, simplified preliminary simulations with detailed, optimization-driven analyses across a wide array of non-residential building types, sizes, and boundary conditions. This two-stage approach drastically reduces computational effort while preserving the depth of insight needed to configure an ICES optimally for each unique case. To identify building types and system configurations most suitably under given boundary conditions, in the first step, the methodology includes systematically simplified preliminary simulations. Detailed optimization calculations were subsequently conducted only for the preselected cases, reducing the computation time from approximately 48 months to less than 4 months. The successful integration of an ICES depends on a relatively high and simultaneous demand for heating and cooling, as this ensures that savings in demand-related costs can offset the initial investment. Simultaneous heating and cooling are particularly advantageous, as they allow the cooling network to act as a direct energy source for the heat pump and facilitate frequent regeneration of the storage tank. Pure air-conditioning loads, however, typically lack sufficient simultaneity, necessitating additional forms of process cooling. Among the evaluated

model buildings, the scenarios that met these requirements included a small and a large school, a large office building and a large hotel.

Future work could extend the developed methodology to other building types, such as data centers or mixed-use districts comprising diverse building types. The integration of waste heat from non-residential buildings with the heating needs of residential buildings offers an opportunity to reduce storage capacity requirements while enhancing system efficiency. Further adaptations could involve considering different climate zones to identify the most suitable locations for ICES applications. Additionally, the model could be expanded to include supplementary system components such as solar thermal collectors, actively cooled photovoltaic modules, or solar air absorbers. This expansion would enable a deeper understanding of how these additional elements influence storage dimensioning and system optimization.

Nomenclature

Abbreviations	
C	including CHP
CC	compression chiller
CEPCI	Chemical Engineering Plant Cost Index
CH	charge
CHP	combined heat and power
DC	dry cooler, discharge
DEU	Germany
EL	electronics store
EU27	European Union average
FC	free cooling
FRA	France
G	excluding CHP
GB	gas boiler
GHL	Green Hospital Lichtenfels
HE CH	heat exchanger charging
HE HP	heat exchanger heat pump
HP	heat pump
ICES	ice energy storage system
IEA	International Energy Agency
NF	non-food
NRB	nonresidential building
orig	measured
PCM	phase change material
syn	simulated
TAO	Technology Alliance of Upper Franconia
VDI	Association of German Engineers
ZET	Center of Energy Technology
(−)	smaller
(o)	standard
(+)	larger
(I)	with ICES
(r)	reference
Symbols	
A_0	investment amount (€)
n	number of data points (−)
$PTPR$	pure time preference rate (%)
Q	energy (MWh)
$\dot{Q}$	power (kW)
R	ratio (−)
R^2	coefficient of determination (−)
Y	value (−)
$\overline{Y}$	mean value (−)
Subscripts and superscripts	
c	cooling
DC	discharge
f,i	model estimated
h	heating
i	actual measured
s	simultaneous

CRediT authorship contribution statement

Marco Griesbach: Writing – review & editing, Writing – original draft, Visualization, Validation, Software, Methodology, Investigation, Formal analysis, Data curation. **Andreas König-Haagen:** Writing – review & editing, Writing – original draft, Formal analysis, Data curation, Conceptualization. **Florian Heberle:** Writing – review & editing, Writing – original draft, Conceptualization. **Dieter Brüggemann:** Writing – review & editing, Writing – original draft, Supervision, Project administration.

Declaration of competing interest

The authors declare that they have no known competing financial interests or personal relationships that could have appeared to influence the work reported in this paper.

Acknowledgments

The authors gratefully acknowledge the financial support of the Bavarian State Ministry of Education, Science and the Arts within the framework Graduiertenkolleg Energieautarke Gebäude of the TechnologieAllianzOberfranken (TAO). Additionally, the authors gratefully acknowledge the financial support of the Upper Franconian Trust (Oberfrankenstiftung) within the framework KomWEisS. Andreas König-Haagen is grateful for the financial support of the Deutsche Forschungsgemeinschaft, (DFG, German Research Foundation) under Grant no KO 6286/1-1.

Data availability

Data will be made available on request.

References

[1] International Energy Agency. World Energy Outlook 2022. IEA, Paris, https://www.iea.org/reports/world-energy-outlook-2022. [Accessed 28 September 2023].
[2] International Energy Agency. Energy Technology Perspectives 2020. IEA, Paris, https://www.iea.org/reports/energy-technology-perspectives-2020. [Accessed 7 September 2021].
[3] International Energy Agency. Tracking Buildings 2020. IEA, Paris, https://www.iea.org/reports/tracking-buildings-2020. [Accessed 7 September 2021].
[4] International Energy Agency. Cooling. IEA, Paris https://www.iea.org/reports/cooling, accessed at 7.September.2021..
[5] International Energy Agency. Is cooling the future of heating 2020. IEA, Paris, https://www.iea.org/commentaries/is-cooling-the-future-of-heating. [Accessed 7 September 2022].
[6] Forman C, Muritala IK, Pardemann R, Meyer B. Estimating the global waste heat potential. Renew Sustain Energy Rev 2016;57(1):1568–79. https://doi.org/10.1016/j.rser.2015.12.192.
[7] Ghoubali R, Byrne P, Miriel J, Bazantay F. Simulation study of a heat pump for simultaneous heating and cooling coupled to buildings. Energy Build 2014;72(5):141–9. https://doi.org/10.1016/j.enbuild.2013.12.047.
[8] Wang S, Qu R, Zhang X, Li Y, Chen J. Thermal performance analysis of ground source heat pump system for low-temperature waste heat recovery storage. Case Stud Therm Eng 2022;35(4):102131. https://doi.org/10.1016/j.csite.2022.102131.
[9] Egging-Bratseth R, Kauko H, Knudsen BR, Bakke SA, Ettayebi A, Haufe IR. Seasonal storage and demand side management in district heating systems with demand uncertainty. Appl Energy 2021;285(2):116392. https://doi.org/10.1016/j.apenergy.2020.116392.
[10] Li H, Hou J, Hong T, Ding Y, Nord N. Energy, economic, and environmental analysis of integration of thermal energy storage into district heating systems using waste heat from data centres. Energy 2021;219(12):119582. https://doi.org/10.1016/j.energy.2020.119582.
[11] Nienborg B, Gschwander S, Munz G, Fröhlich D, Helling T, Horn R, et al. Life cycle assessment of thermal energy storage materials and components. Energy Proc 2018;155:111–20. https://doi.org/10.1016/j.egypro.2018.11.063.
[12] Shipper K. Demonstration ice storage with waste heat recovery project: final report. Austin, Texas: The Council; 1980.
[13] Philippen D, Carbonell D, Battaglia M, Thissen B, Kunath L. Validation of an ice storage model and its integration into a solar-ice system. EuroSun 2018 Conference Proceedings 2018:1–12. https://doi.org/10.18086/eurosun2018.13.12.
[14] Winteler C, Dott R, Afjei T, Hafner B. Seasonal performance of a combined solar, heat pump and latent heat storage system. Energy Proc 2014;48:689–700. https://doi.org/10.1016/j.egypro.2014.02.080.
[15] Hollmuller P, Oliveira F de, Graf O, Thiele W. Solar assisted heat pump with ice storage for a 19'000 m^2 retrofitted multi-family building complex. Energy Proc 2017;122:271–6. https://doi.org/10.1016/j.egypro.2017.07.321.
[16] Carbonell D, Philippen D, Granzotto M, Haller MY. Simulation of a solar-ice system for heating applications. System validation with one-year of monitoring data.

Energy Build 2016;127(5):846–58. https://doi.org/10.1016/j.enbuild.2016.06.058.
[17] Rismanchi B, Saidur R, Masjuki HH, Mahlia TMI. Thermodynamic evaluation of utilizing different ice thermal energy storage systems for cooling application in office buildings in Malaysia. Energy Build 2012;53:117–26. https://doi.org/10.1016/j.enbuild.2012.06.013.
[18] Wu C-T, Tsai Y-H. Design of an ice thermal energy storage system for a building of hospitality operation. Int J Hospit Manag 2015;46:46–54. https://doi.org/10.1016/j.ijhm.2015.01.005.
[19] Song X, Zhu T, Liu L, Cao Z. Study on optimal ice storage capacity of ice thermal storage system and its influence factors. Energy Convers Manag 2018;164:288–300. https://doi.org/10.1016/j.enconman.2018.03.007.
[20] Zhu P, Zheng JH, Li Z, Wu QH, Wang L. Optimal operation for district cooling systems coupled with ice storage units based on the per-unit value form. Energy 2024;302(3):131730. https://doi.org/10.1016/j.energy.2024.131730.
[21] Cao H, Lin J, Li N. Optimal control and energy efficiency evaluation of district ice storage system. Energy 2023;276(3):127598. https://doi.org/10.1016/j.energy.2023.127598.
[22] Chan A, Chow T, Fong S, Lin J. Performance evaluation of district cooling plant with ice storage. Energy 2006;31(14):2750–62. https://doi.org/10.1016/j.energy.2005.11.022.
[23] Griesbach M, König-Haagen A, Brüggemann D. Numerical analysis of a combined heat pump ice energy storage system without solar benefit – analytical validation and comparison with long term experimental data over one year. Appl Therm Eng 2022;213(1):118696. https://doi.org/10.1016/j.applthermaleng.2022.118696.
[24] Griesbach M, König-Haagen A, Heberle F, Brüggemann D. Multi-criteria assessment and optimization of ice-energy storage systems in combined heat and cold supply networks of a campus building. Energy Convers Manag 2023;287(1):117118. https://doi.org/10.1016/j.enconman.2023.117118.
[25] Henn S, Richarz J, Maier L, Ying X, Osterhage T, Mehrfeld P, et al. Influences of usage intensity and weather on optimal building energy system design with multiple storage options. Energy Build 2022;270(5):112222. https://doi.org/10.1016/j.enbuild.2022.112222.
[26] Zentrum für Umweltbewusstes Bauen e.V. Entwicklung einer Datenbank mit Modellgebäuden für energiebezogene Untersuchungen, insbesondere der Wirtschaftlichkeit (in German). Kassel https://www.bbsr.bund.de/BBSR, accessed at 12.April.2022..
[27] Wirtz M. nPro: a web-based planning tool for designing district energy systems and thermal networks. Energy 2023;268(4):126575. https://doi.org/10.1016/j.energy.2022.126575.
[28] Hoerner M, Cischinsky H, Bischof J, Schwarz S, Meinel G, Busch R. Forschungsdatenbank nichtwohngebäude (in German). Darmstadt: IWU: enob: datanwg schlussbericht. 2022.
[29] Landkreis Lichtenfels im Rahmen einer Kooperation der Technologie Allianz Oberfranken. Abschlussbericht Green Hospital Lichtenfels 2022 (in German). Hof.
[30] Versteeg HK, Malalasekera W. An introduction to computational fluid dynamics: the finite volume method. Harlow England, New York: Pearson Education Ltd; 2007.
[31] Comini G, Del Guidice S, Lewis RW, Zienkiewicz OC. Finite element solution of non-linear heat conduction problems with special reference to phase change. Int J Numer Methods Eng 1974;8(3):613–24. https://doi.org/10.1002/nme.1620080314.
[32] Rösler F, Brüggemann D. Shell-and-tube type latent heat thermal energy storage: numerical analysis and comparison with experiments. Heat Mass Tran 2011;47(8):1027–33. https://doi.org/10.1007/s00231-011-0866-9.
[33] Schiesser WE. The numerical method of lines: integration of partial differential equations. Bethlehem, Pennsylvania: Academic Press Elsevier Science; 1991.
[34] Patankar SV. Numerical heat transfer and fluid flow. Boca Raton, Florida: CRC Press; 1980.
[35] Seban RA, McLaughlin EF. Heat transfer in tube coils with laminar and turbulent flow. Int J Heat Mass Tran 1963;6(5):387–95. https://doi.org/10.1016/0017-9310(63)90100-5.
[36] Churchill SW, Chu HHS. Correlating equations for laminar and turbulent free convection from a horizontal cylinder. Int J Heat Mass Tran 1975;18(9):1049–53. https://doi.org/10.1016/0017-9310(75)90222-7.
[37] Kusuda T, Achenbach PR. Earth temperature and thermal diffusivity at selected stations in the United States. ASHRAE Transactions 1965;71(1):61–74.
[38] König-Haagen A, Franquet E, Faden M, Brüggemann D. A study on the numerical performances of diffuse interface methods for simulation of melting and their practical consequences. Energies 2021;14(2):354. https://doi.org/10.3390/en14020354.
[39] Voller VR. An overview of numerical methods for solving phase change problems. Advances in numerical heat transfer 1997;1(9):341–80.
[40] The MathWorks Inc. Matlab ® release 2020b. 2020. Natick, Massachusetts, USA.
[41] The MathWorks Inc. Simulink ® release 2020b. 2020. Natick, Massachusetts, USA.
[42] Solar-Institut Jülich. CARNOT toolbox ver. 6.3 for matlab/simulink 2016b. 2018. Jülich, Deutschland.
[43] Schwamberger K. Modellbildung und Regelung von Gebäudeheizungsanlagen mit Wärmepumpen. Düsseldorf: VDI-Verlag; 1991.
[44] DIN 8900-6:1987-12. Wärmepumpen; Anschlußfertige Heiz-Wärmepumpen mit elektrisch angetriebenen Verdichtern. Berlin: Beuth Verlag; 1987.
[45] Wischhusen S. Dynamische Simulation zur wirtschaftlichen Bewertung von komplexen Energiesystemen. Göttingen: Cuvillier: Dissertation; 2005.
[46] Association of German engineers. VDI 2067 part 1: economic efficiency of building installations - fundamentals and economic calculation. Berlin: Beuth Verlag; 2012.
[47] Vivian J, Heer P, Fiorentini M. Optimal sizing and operation of seasonal ice thermal storage systems. Energy Build 2023;300:113633. https://doi.org/10.1016/j.enbuild.2023.113633.
[48] Berger M, Schroeteler B, Sperle H, Püntener P, Felder T, Worlitschek J. Assessment of residential scale renewable heating solutions with thermal energy storages. Energy 2022;244(11):122618. https://doi.org/10.1016/j.energy.2021.122618.
[49] Chemical Engineering. The Chemical Engineering Plant Cost Index https://www.chemengonline.com/pci-home, accessed at 5.April.2022..
[50] Tribe MA, Alpine RLW. Scale economies and the “0.6 rule”. Eng Costs Prod Econ 1986;10(1):271–8. https://doi.org/10.1016/0167-188X(86)90053-4.
[51] Wang J, Zhai Z, Jing Y, Zhang C. Particle swarm optimization for redundant building cooling heating and power system. Appl Energy 2010;87(12):3668–79. https://doi.org/10.1016/j.apenergy.2010.06.021.
[52] Umweltbundesamt. Methodenkonvention 3.1 zur Ermittlung von Umweltkosten - Kostensätze. Dessau-Roßlau; 2020 (in German), https://www.umweltbundesamt.de/sites/default/files/medien/1410/publikationen/2020-12-21_methodenkonvention_3_1_kostensaetze.pdf. [Accessed 12 April 2022].
[53] Waldhoff S, Anthoff D, Rose S, Tol RSJ. The marginal damage costs of different greenhouse gases: an application of FUND. Economics 2014;8(1). https://doi.org/10.5018/economics-ejournal.ja.2014-31.
[54] Wang J-J, Fu C, Yang K, Zhang X-T, Shi G-h, Zhai J. Reliability and availability analysis of redundant BCHP (building cooling, heating and power) system. Energy 2013;61:531–40. https://doi.org/10.1016/j.energy.2013.09.018.
[55] Nelder JA, Mead R. A simplex method for function minimization. Comput J 1965;7(4):308–13. https://doi.org/10.1093/comjnl/7.4.308.
[56] nPro Energy GmbH. nPro. Erkelenz. 2023. Deutschland.
[57] Association of German Engineers. VDI 3807 part 1: characteristic consumption values for buildings - fundamentals. Berlin: Beuth Verlag; 2013.
[58] Wang Y, Li B. An optimized solar-air degree-day method to evaluate energy demand for poultry buildings in different climate zones. Front Agr Sci Eng 2020;7(4):478. https://doi.org/10.15302/J-FASE-2019289.
[59] Sha H, Xu P, Hu C, Li Z, Chen Y, Chen Z. A simplified HVAC energy prediction method based on degree-day. Sustain Cities Soc 2019;51:101698. https://doi.org/10.1016/j.scs.2019.101698.
[60] Verbai Z, Lakatos Á, Kalmár F. Prediction of energy demand for heating of residential buildings using variable degree day. Energy 2014;76(1):780–7. https://doi.org/10.1016/j.energy.2014.08.075.
[61] Wirtz M, Hahn M, Schreiber T, Müller D. Design optimization of multi-energy systems using mixed-integer linear programming: which model complexity and level of detail is sufficient? Energy Convers Manag 2021;240(4):114249. https://doi.org/10.1016/j.enconman.2021.114249.